Collective rotation and vibration in neutron-rich ^{180,182}Hf nuclei

E. Ngijoi-Yogo,[*] S. K. Tandel, G. Mukherjee,[†] I. Shestakova, and P. Chowdhury[‡]
Department of Physics, University of Massachusetts Lowell, Lowell, Massachusetts 01854, USA

C. Y. Wu,[§] D. Cline, A. B. Hayes, and R. Teng
Nuclear Structure Research Laboratory, University of Rochester, Rochester, New York 14627, USA

R. M. Clark, P. Fallon, A. O. Macchiavelli, and K. Vetter[§]
Nuclear Science Division, Lawrence Berkeley National Laboratory, Berkeley, California 94720, USA

F. G. Kondev
Argonne National Laboratory, Argonne, Illinois 60439, USA

S. Langdown and P. M. Walker
Department of Physics, University of Surrey, Guildford GU2 7XH, United Kingdom

C. Wheldon[‖]
Department of Physics, Oliver Lodge Laboratory, University of Liverpool, Liverpool L69 7ZE, United Kingdom

D. M. Cullen
Department of Physics and Astronomy, University of Manchester, Manchester M13 9PL, United Kingdom
(Received 14 July 2006; revised manuscript received 11 January 2007; published 15 March 2007)

High-spin states in neutron-rich ^{180}Hf and ^{182}Hf nuclei were populated through inelastic and transfer reactions with a ^{136}Xe beam incident on a thin ^{180}Hf target, and investigated using particle-γ coincidence techniques. New collective band structures were observed, and previously known rotational and vibrational bands in these nuclei were extended to higher angular momenta. No obvious nucleon alignment was observed in the ground state band of either nucleus up to $\hbar\omega = 0.43$ MeV, a significant delay compared to lighter even-even Hf isotopes. Woods-Saxon cranking calculations were performed to predict the nature of the first band crossings and shape evolution in ^{180,182}Hf.

DOI: 10.1103/PhysRevC.75.034305 PACS number(s): 21.10.Re, 21.60.Ev, 23.20.Lv, 27.70.+q

I. INTRODUCTION

Nuclei in the $A \approx 180$ region exhibit axially symmetric prolate deformations in their ground state. The low-lying excited states of these nuclei are therefore characterized by collective rotational bands. Furthermore, near their respective Fermi levels, both protons and neutrons have available high-j orbitals with large projections (Ω) along the symmetry axis. This stimulates competition along the yrast line between collective angular momentum perpendicular to the symmetry axis and particle angular momentum aligned along the symmetry axis. The interplay and changing dominance between collective and noncollective modes of excitations as a function of angular momentum remains a key focus of nuclear structure investigations.

Hafnium ($Z = 72$) nuclei have long been considered to be prototypical systems for the observation of these competing effects. The motivation for the present study of neutron-rich hafnium nuclei is twofold. Our recent investigations of these nuclei [1,2] have focused on the population and decay of high-K isomers ($K = \Sigma_i \Omega_i$), corroborating earlier theoretical predictions [3] that multiquasiparticle excitations would be increasingly favored in neutron-rich isotopes. Interestingly, other theoretical calculations predict a transition from prolate to oblate shapes along the yrast line at higher spins [4,5] for these same neutron-rich hafnium nuclei. Since the only data collected in our earlier experiments were between beam pulses, all collective excitations observed were those that were fed via isomer decays and not those directly populated in the reactions. An additional motivation was to complement our earlier work on multiquasiparticle isomers by a careful characterization of previously bypassed two-quasiparticle low-K rotational structures, which form the building blocks of the high-K excitations. The present work focuses specifically on the experimental identification and characterization of collective structures in ^{180,182}Hf. The new results extend the experimental information in these nuclei to significantly higher

[*]Present address: Department of Physics and Astronomy, Mississippi State University, Mississippi State, Mississippi 39762, USA.
[†]Present address: Variable Energy Cyclotron Centre, Kolkata 700064, India.
[‡]Corresponding author: partha_chowdhury@uml.edu.
[§]Present address: Lawrence Livermore National Laboratory, Livermore, California 94551, USA.
[‖]Present address: Hahn-Meitner-Institute, Glienicker Strasse 100, D-14109 Berlin, Germany

angular momenta (factors of 1.5 and 2 for ^{180}Hf and ^{182}Hf, respectively). Both rotational and vibrational structures exhibit unusual characteristics at high spin. A detailed analysis of the extended systematics of quasiparticle alignments in these neutron-rich systems has been performed, and results are discussed within the framework of cranked Woods-Saxon calculations.

II. EXPERIMENTAL DETAILS

Populating high-spin states in neutron-rich nuclei in this mass region is experimentally challenging. Fusion-evaporation techniques fail, since stable beam-target combinations tend to preferentially form fused systems on the neutron-deficient side of the valley of stability. The relatively new technique of utilizing inelastic and transfer reactions with heavy beams [6] has proved to be quite effective in our recent studies [1,2]. In the present work, excited states in ^{180,182}Hf were populated with a 750 MeV ^{136}Xe beam, incident on a thin ^{180}Hf target (410 μg/cm^2, isotopic purity $> 94\%$) backed by a 40 μg/cm^2 carbon foil. The beam ($\approx 15\%$ above the Coulomb barrier) was provided by the 88-in. cyclotron at the Lawrence Berkeley National Laboratory. Emitted γ rays were detected by the GAMMASPHERE (GS) array consisting of 100 large-volume Compton-suppressed high-purity germanium (HPGe) detectors. The excited nuclei were allowed to recoil out of the thin target into vacuum, with a well-defined velocity measured by their time of flight. The beamlike and targetlike fragments were detected and identified with CHICO, a position-sensitive parallel-plate avalanche counter [7]. The master trigger was the coincident detection of at least two γ rays in GS and two correlated particles in CHICO. With a beam intensity averaging 2.5 pnA, approximately 5.3×10^8 raw events were collected.

The measurements of position and time-of-flight difference with CHICO were used to distinguish between beamlike and targetlike fragments following inelastic excitation or transfer. The measured velocity and angle were used to reconstruct the particle kinematics event by event, and the prompt transitions emitted by nuclei decaying in flight were corrected for Doppler shifts (Fig. 1). The events were sorted with the TSCAN software package [8] into coincident two-dimensional matrices and three-dimensional cubes. The matrices and cubes were analyzed, and level schemes constructed using the ESCL8R and LEVIT8R programs in the RADWARE package [9].

The method of directional angular correlations from oriented states (DCO) [10,11] was applied to establish the multipolarity of transitions and assign level spins for the collective bands observed in the inelastic channel ^{180}Hf. A matrix was constructed with γ rays detected at $90^\circ \pm 10^\circ$ with respect to the direction of the emitting recoils on one axis and those detected at $30^\circ/150^\circ \pm 10^\circ$ with respect to the particle directions on the other. The experimental DCO ratio $R_{\mathrm{DCO}}(\gamma)$ of a γ transition was calculated as

$$R_{\mathrm{DCO}}(\gamma) = \frac{I_\gamma(30^\circ/150^\circ, 90^\circ)}{I_\gamma(90^\circ, 30^\circ/150^\circ)}, \qquad (1)$$

where $I_\gamma(\theta_1, \theta_2)$ is the intensity of the γ transition observed at an angle θ_1, in coincidence with a stretched $E2$ transition observed at an angle θ_2. Tentative parity assignments of new bands were based on intensity balance considerations, observed branching ratios, and systematics of similar structures in neighboring isotopes.

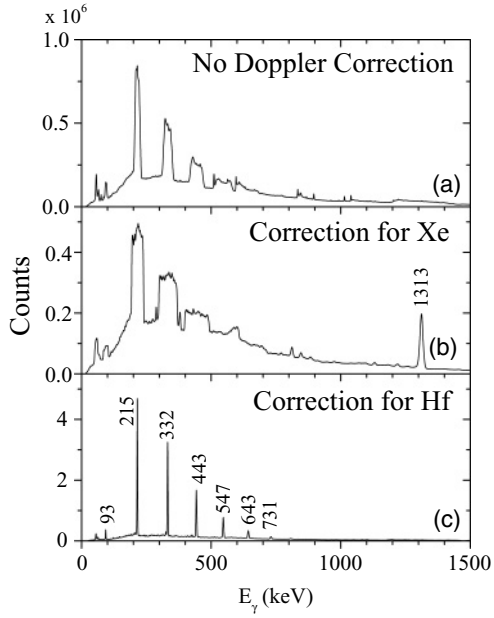

FIG. 1. Effect of Doppler correction on spectra. Lines are sharpened when the correction for the appropriate recoiling ion is applied and broadened if the correction for the reaction partner is applied (see labeled peaks).

III. RESULTS

A. Band structures in ^{180}Hf

The level scheme of ^{180}Hf deduced from the present work is shown in Fig. 2. Energies, relative γ-ray intensities, and the proposed multipolarity assignments for the observed γ rays are presented in Table I. Intensities were normalized to 1000 for the 332-keV $6^+ \rightarrow 4^+$ transition. The spin alignment of a nucleus excited through a binary reaction above Coulomb barrier energies is complex, and systematic variations in the DCO ratios were observed for nonsuccessive transitions in a cascade. For successive transitions in a cascade, with a stretched $E2$ transition in the ground state band as one of the gating transitions, values of R_{DCO} are observed to cluster around the expected values of 1.0 and 0.5 for stretched quadrupole and dipole transitions, respectively. Measured DCO ratios, using this prescription, are included in the table for all clean γ rays that are statistically significant and help in assigning spins and parities to observed band structures. While the statistical uncertainties are small, measuring angles with respect to the recoil direction leads to different Doppler broadening at the two chosen angle bins, as well as event-by-event variations in the detection efficiencies, depending on how many detectors make the particular angle bin. These normalization uncertainties limited the DCO ratios that could be extracted from the data. For nonstretched and mixed-multipolarity transitions, other complementary information needed to be also considered for final spin assignments.

TABLE I. Energies, initial and final states, and intensities for the γ-ray transitions observed in ^{180}Hf. DCO ratios are included wherever reliable, statistically significant values were measurable. Uncertainties in the transition energies are $\sim \pm 0.5$ keV. Transition energies above 1000 keV are quoted to the nearest integer.

E_γ(keV)	Band$_i$ $\rightarrow$ Band$_f$	E_i(keV)	$I_i^\pi \rightarrow I_f^\pi$	I_γ	R_{DCO}
57.8	1 $\rightarrow$ GSB	1141	$8^- \rightarrow 8^+$		
92.8	GSB $\rightarrow$ GSB	93	$2^+ \rightarrow 0^+$	231(8)	
108.2	6 $\rightarrow$ 5	1482	$5^- \rightarrow 4^-$	6.7(4)	
129.7	5 $\rightarrow$ 6	1612	$6^- \rightarrow 5^-$	2.07(9)	
152.2	6 $\rightarrow$ 5	1764	$7^- \rightarrow 6^-$	1.3(2)	
173.0	5 $\rightarrow$ 6	1937	$8^- \rightarrow 7^-$	0.7(1)	
186.6	9 $\rightarrow$ 9	1370	$4^+ \rightarrow 2^+$		
192.0	4 $\rightarrow$ 3	1894	$7^+ \rightarrow 6^+$		
196.2	6 $\rightarrow$ 5	2133	$9^- \rightarrow 8^-$	0.4(1)	
209(1)	7 $\rightarrow$ 7	1408	$4^+ \rightarrow 2^+$		
215.3	GSB $\rightarrow$ GSB	308	$4^+ \rightarrow 2^+$	1070(35)	
216.2	5 $\rightarrow$ 6	2349	$10^- \rightarrow 9^-$		
218.3	3 $\rightarrow$ 4	2112	$8^+ \rightarrow 7^+$	2.3(1)	
238.1	5 $\rightarrow$ 5	1612	$6^- \rightarrow 4^-$	3.6(1)	
241.0	4 $\rightarrow$ 3	2353	$9^+ \rightarrow 8^+$	1.9(1)	
242.9	2 $\rightarrow$ 1	1384	$9^- \rightarrow 8^-$	14.4(4)	
263.0	3 $\rightarrow$ 4	2616	$10^+ \rightarrow 9^+$	1.1(1)	
266.1	8 $\rightarrow$ 8	1557	$5^+ \rightarrow 3^+$		
268.1	1 $\rightarrow$ 2	1652	$10^- \rightarrow 9^-$	12.4(2)	
282.0	4 $\rightarrow$ 3	2898	$11^+ \rightarrow 10^+$	0.4(1)	
282.3	6 $\rightarrow$ 6	1764	$7^- \rightarrow 5^-$	4.6(2)	
288.4	9 $\rightarrow$ 9	1658	$6^+ \rightarrow 4^+$		
293.0	2 $\rightarrow$ 1	1945	$11^- \rightarrow 10^-$	5.9(1)	
294.5	3 $\rightarrow$ 4	3193	$12^+ \rightarrow 11^+$		
314.8	7 $\rightarrow$ 7	1723	$6^+ \rightarrow 4^+$	5.3(5)	
316.9	1 $\rightarrow$ 2	2262	$12^- \rightarrow 11^-$	2.7(1)	
325.3	5 $\rightarrow$ 5	1937	$8^- \rightarrow 6^-$	2.7(2)	
332.2	GSB $\rightarrow$ GSB	640	$6^+ \rightarrow 4^+$	1000(30)	1.12(2)
340.6	2 $\rightarrow$ 1	2603	$13^- \rightarrow 12^-$	1.4(1)	
362.3	1 $\rightarrow$ 2	2965	$14^- \rightarrow 13^-$	0.6(1)	
369.1	6 $\rightarrow$ 6	2133	$9^- \rightarrow 7^-$	2.5(4)	
371.1	10 $\rightarrow$ 10	2272	$(8^+) \rightarrow (6^+)$	0.8(2)	
371.2	8 $\rightarrow$ GSB	1928	$7^+ \rightarrow 5^+$	5.1(3)	
384.8	2 $\rightarrow$ 1	3350	$15^- \rightarrow 14^-$	0.3(1)	
388.1	9 $\rightarrow$ 9	2046	$8^+ \rightarrow 6^+$	3.2(3)	
396.8	11 $\rightarrow$ 11	2300		3.6(3)	
405.4	1 $\rightarrow$ 2	3755	$16^- \rightarrow 15^-$	0.2(1)	
409.0	7 $\rightarrow$ 7	2132	$8^+ \rightarrow 6^+$	10.2(6)	
409.9	3 $\rightarrow$ 3	2112	$8^+ \rightarrow 6^+$	0.4(1)	
412.2	5 $\rightarrow$ 5	2349	$10^- \rightarrow 8^-$	2.0(1)	
424.8	2 $\rightarrow$ 1	4180	$17^- \rightarrow 16^-$		
443.4	GSB $\rightarrow$ GSB	1083	$8^+ \rightarrow 6^+$	519(15)	1.16(2)
453.8	6 $\rightarrow$ 6	2587	$11^- \rightarrow 9^-$	1.5(1)	
456.7	10	2729	$(10^+) \rightarrow (8^+)$	2.7(2)	
459.0	4 $\rightarrow$ 4	2353	$9^+ \rightarrow 7^+$	0.8(1)	
470.4	8 $\rightarrow$ 8	2398	$9^+ \rightarrow 7^+$	2.1(2)	
480.3	7 $\rightarrow$ 7	2613	$10^+ \rightarrow 8^+$	5.3(4)	
485.2	9 $\rightarrow$ 9	2531	$10^+ \rightarrow 8^+$	1.4(3)	
495.1	11 $\rightarrow$ 11	2795		0.9(2)	
498.0	5 $\rightarrow$ 5	2847	$12^- \rightarrow 10^-$	0.9(1)	
501.4	1 $\rightarrow$ GSB	1141	$8^- \rightarrow 6^+$		
504.0	3 $\rightarrow$ 3	2616	$10^+ \rightarrow 8^+$	0.7(1)	
511.2	1 $\rightarrow$ 1	1652	$10^- \rightarrow 8^-$	1.3(2)	
515.4	7 $\rightarrow$ 7	3128	$12^+ \rightarrow 10^+$	1.7(2)	

TABLE I. *(Continued.)*

E_γ(keV)	Band$_i$ → Band$_f$	E_i(keV)	$I_i^\pi \rightarrow I_f^\pi$	I_γ	R_{DCO}
535.4	6 → 6	3122	$13^- \rightarrow 11^-$	0.7(2)	
545.0	4 → 4	2898	$11^+ \rightarrow 9^+$	0.5(1)	
547.3	GSB → GSB	1630	$10^+ \rightarrow 8^+$	245(6)	1.12(2)
548.9	7 → 7	3676	$14^+ \rightarrow 12^+$	1.3(2)	
560.9	2 → 2	1945	$11^- \rightarrow 9^-$	0.8(2)	
561.7	8 → 8	2959	$11^+ \rightarrow 9^+$	1.0(1)	
569.8	10 → 10	3299	$(12^+) \rightarrow (10^+)$	1.8(2)	
576.7	3 → 3	3193	$12^+ \rightarrow 10^+$		
577.8	9 → 9	3109	$12^+ \rightarrow 10^+$	0.4(2)	
583.7	5 → 5	3431	$14^- \rightarrow 12^-$		
588.0	11 → 11	3383			
592.3	7 → 7	4268	$16^+ \rightarrow 14^+$	0.5(2)	
596.7	10 → 7	2729	$(10^+) \rightarrow 8^+$	1.1(2)	
610.0	1 → 1	2262	$12^- \rightarrow 10^-$	1.0(1)	
610.6	6 → 6	3733	$15^- \rightarrow 13^-$		
643.4	GSB → GSB	2273	$12^+ \rightarrow 10^+$	101(4)	1.06(2)
645.8	8 → 8	3605	$13^+ \rightarrow 11^+$	0.5(1)	
657.5	2 → 2	2603	$13^- \rightarrow 11^-$	0.6(1)	
659.2	5 → 5	4090	$16^- \rightarrow 14^-$		
670.8	9 → 9	3780	$14^+ \rightarrow 12^+$	0.4(2)	
671.0	10 → 10	3970	$(14^+) \rightarrow (12^+)$		
679.1	6 → 6	4412	$17^- \rightarrow 15^-$		
686.8	10 → 7	3299	$(12^+) \rightarrow 10^+$	0.9(2)	
703.0	1 → 1	2965	$14^- \rightarrow 12^-$	0.5(1)	
730.9	GSB → GSB	3004	$14^+ \rightarrow 12^+$	32.5(3)	1.03(2)
747.2	2 → 2	3350	$15^- \rightarrow 13^-$	0.3(3)	
776.1	9 → GSB	3780	$14^+ \rightarrow 14^+$		
790.0	1 → 1	3755	$16^- \rightarrow 14^-$		
807.9	GSB → GSB	3812	$16^+ \rightarrow 14^+$	7.8(2)	0.98(3)
829.8	2 → 2	4180	$17^- \rightarrow 15^-$		
836.3	9 → GSB	3109	$12^+ \rightarrow 12^+$	0.7(1)	
844.9	8 → GSB	1928	$7^+ \rightarrow 8^+$	0.7(1)	
868.5	GSB → GSB	4681	$18^+ \rightarrow 16^+$	1.3(1)	
902.4	9 → GSB	2531	$10^+ \rightarrow 10^+$	1.0(1)	
916.1	8 → GSB	1557	$5^+ \rightarrow 6^+$	2.2(2)	
962.9	9 → GSB	2046	$8^+ \rightarrow 8^+$	1.7(2)	
965.7	10 → GSB	3970	$(14^+) \rightarrow 14^+$		
983.0	7 → GSB	2613	$10^+ \rightarrow 10^+$	1.8(3)	
983.4	8 → GSB	1291	$3^+ \rightarrow 4^+$	5.7(3)	
1018	9 → GSB	1658	$6^+ \rightarrow 6^+$	3.1(2)	1.05(6)
1026	10 → GSB	3299	$(12^+) \rightarrow 12^+$		
1050	7 → GSB	2132	$8^+ \rightarrow 8^+$	8.9(2)	0.69(3)
1062	3 → GSB	1702	$6^+ \rightarrow 6^+$	3.1(2)	
1065	5 → GSB	1374	$4^- \rightarrow 4^+$		
1083	7 → GSB	1723	$6^+ \rightarrow 6^+$	13.6(3)	0.72(3)
1098	10 → GSB	2729	$(10^+) \rightarrow 10^+$	5.8(4)	0.91(5)
1100	7 → GSB	1408	$4^+ \rightarrow 4^+$	23(2)	
1106	7 → GSB	1199	$2^+ \rightarrow 2^+$	11.3(3)	
1110	11 → GSB	3383	$\rightarrow 10^+$		
1165	11 → GSB	2795	$\rightarrow 10^+$		
1189	10 → GSB	2272	$(8^+) \rightarrow 8^+$	7.0(4)	
1198	8 → GSB	1291	$3^+ \rightarrow 2^+$	31(2)	
1217	11 → GSB	2300	$\rightarrow 8^+$		
1249	8 → GSB	1557	$5^+ \rightarrow 4^+$	16.5(8)	
1261	10 → GSB	1901	$(6^+) \rightarrow 6^+$	1.6(2)	
1263	11 → GSB	1903	$\rightarrow 6^+$	3.6(3)	
1288	8 → GSB	1928	$7^+ \rightarrow 6^+$	10.0(5)	0.62(3)

TABLE I. *(Continued.)*

E_γ(keV)	Band$_i$ → Band$_f$	E_i(keV)	$I_i^\pi \rightarrow I_f^\pi$	I_γ	$R_{\rm DCO}$
1315	8 → GSB	2398	$9^+ \rightarrow 8^+$	4.4(2)	0.62(4)
1315	7 → GSB	1408	$4^+ \rightarrow 2^+$	13.5(5)	
1330	8 → GSB	2959	$11^+ \rightarrow 10^+$	2.1(2)	
1332	8 → GSB	3605	$13^+ \rightarrow 12^+$	0.6(1)	
1350	9 → GSB	1658	$6^+ \rightarrow 4^+$	0.7(1)	
1394	3 → GSB	1702	$6^+ \rightarrow 4^+$	4.0(5)	
1404	7 → GSB	3676	$14^+ \rightarrow 12^+$		
1415	7 → GSB	1723	$6^+ \rightarrow 4^+$	14.0(2)	1.07(3)
1493	7 → GSB	2132	$8^+ \rightarrow 6^+$	13.5(2)	1.07(3)
1498	7 → GSB	3128	$12^+ \rightarrow 10^+$	2.8(2)	1.02(5)
1530	7 → GSB	2613	$10^+ \rightarrow 8^+$	4.7(4)	1.01(4)
1669	10 → GSB	3299	$(12^+) \rightarrow 10^+$		

1. The ground state band

Representative spectra for the ground state band (GSB) are shown in Fig. 3. The upper panel shows the spectrum obtained from the sum of single-gated spectra of the GSB transitions. This band was known only up to $I^\pi = 12^+$ prior to this work [12] and has been extended to 18^+. The 869-keV γ ray, the highest transition placed in the GSB, is clearly observed in the spectrum double-gated on the 731- and 808-keV transitions. The rapid drop in the transition intensities prevented the observation of any higher-lying excited state. The measured DCO ratios of the stretched quadrupole GSB transitions range between 0.98 and 1.16.

2. Bands 1 and 2

Bands 1 and 2 are signature partners built on the 1141-keV $I^\pi = 8^-$ isomeric state ($t_{1/2} = 5.5$ hr). Low-lying states of bands 1 and 2 were known from previous out-of-beam decay spectroscopy [1]. These have been extended from 12^- to 16^- and from 11^- to 17^-, respectively, with six new $\Delta I = 1$ transitions between the signature partners (Fig. 4). The band intensities were ∼1.5% of the strongest GSB transition.

3. Bands 3 and 4

Bands 3 and 4, signature partners built on a 1702-keV bandhead, were observed previously [13,14] and assigned a tentative spin-parity of 6^+ for the bandhead. The bands were identified in the present study without extension. The previously observed dominance of the $\Delta I = 1$ transition intensities over the $\Delta I = 2$ transition intensities in the band is corroborated (Fig. 5). The overall γ-ray intensity of these bands is less than 0.5% of the strongest GSB transition. While the bandhead had been determined previously to be isomeric, no noticeable difference in coincident intensities across the bandhead was observed on varying the width of the coincidence time window. This suggests an upper limit of ∼5 ns (the time resolution of the detectors) for the half-life of the bandhead. It was not possible to extract reliable DCO ratios for the 1062- and 1394-keV transitions from the isomeric bandhead to the 6^+ and 4^+ states of the GSB. Nevertheless, the absence of a decay branch to the 2^+ state of the GSB limits the possible spin of the bandhead to 5 or 6. Furthermore, the isomeric nature of the low-lying bandhead, which necessarily implies a two-quasiparticle configuration

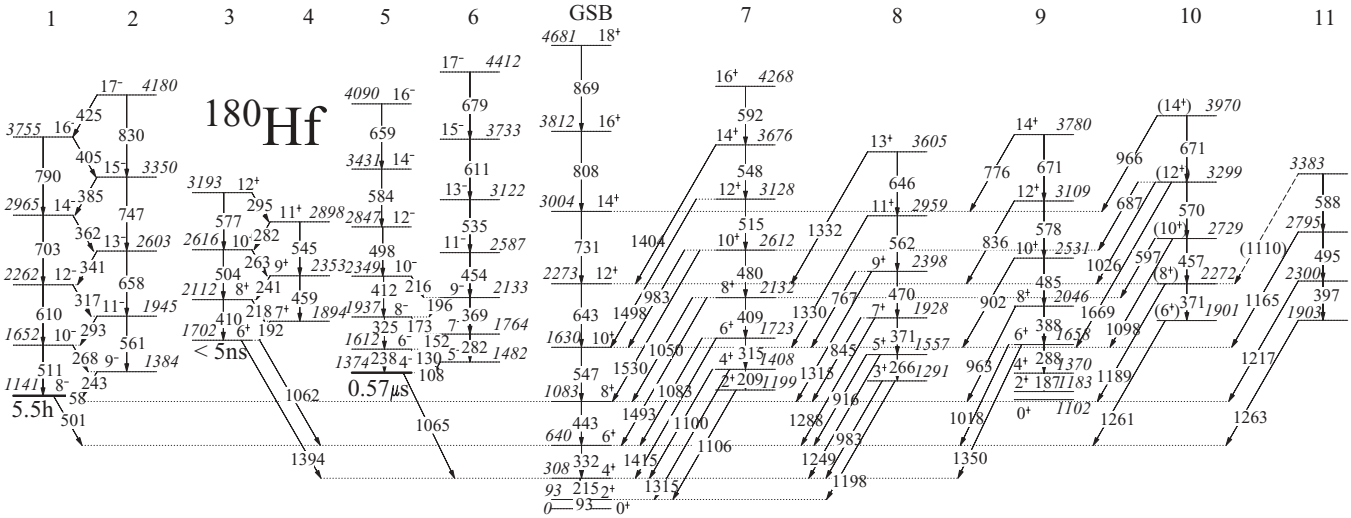

FIG. 2. Decay scheme of ^{180}Hf deduced from the present work. All energies are in keV. Half-lives are quoted for three high-K bandheads.

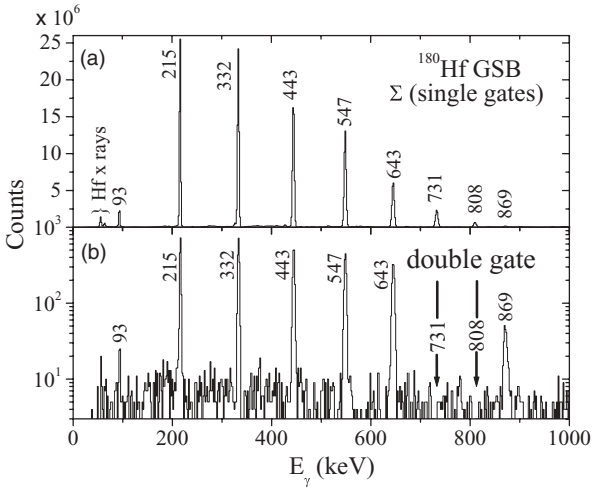

FIG. 3. γ-ray coincidence spectra showing transitions in the ground state band of ^{180}Hf. (a) Sum of spectra single-gated on the band members. (b) Spectrum obtained from a double gate on 731- and 808-keV transitions to show more clearly the highest observed 869-keV transition.

in an even-even nucleus, together with a scrutiny of both the available valence orbitals in this nucleus as well as the systematics of two-quasiparticle bandheads in neighboring nuclei, effectively constrains the bandhead to the earlier spin-parity assignment of 6^+.

4. Bands 5 and 6

Bands 5 and 6 are signature partners built on the 1374-keV $I^\pi = 4^-$ isomeric state with $t_{1/2} = 0.57$ μs. These have been extended to 16^- and 17^-, from previously known I^π values of 12^- and 13^-, respectively [12,15]. The $\Delta I = 2$ transitions dominate in intensity over the $\Delta I = 1$ transitions for this band (Fig. 6). No new $\Delta I = 1$ transitions were observed between the partners. These two bands are approximately 0.5–1% as intense as the strongest GSB transition.

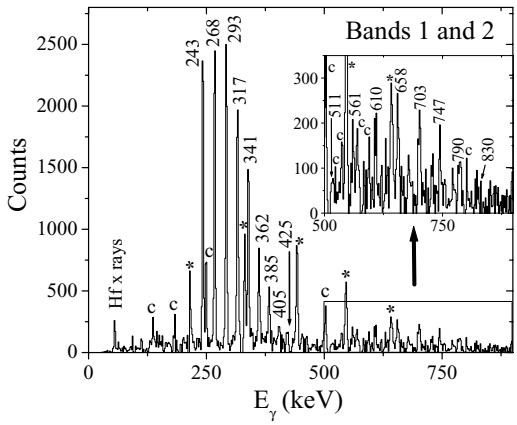

FIG. 4. Summed coincidence spectra double-gated on transitions in bands 1 and 2 of ^{180}Hf. Remnants of the strong GSB transitions from a slight under-subtraction of background are marked with a (*) and contaminants with a (c). The $E2$ transitions, shown in the inset, are weaker than the $\Delta I = 1$ transitions.

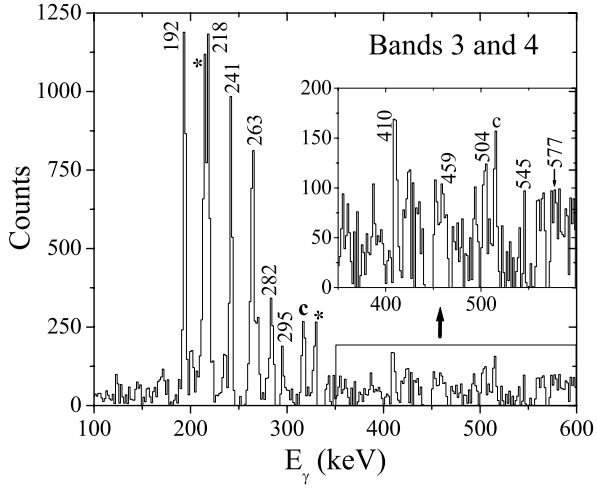

FIG. 5. Summed coincidence spectra double-gated on transitions in bands 3 and 4 of ^{180}Hf. Transitions in the GSB are marked with a (*) and contaminants with a (c). $\Delta I = 1$ transitions in the band are stronger than $E2$ transitions shown in the inset.

5. Bands 7 and 8

Bands 7 and 8 were previously reported as signature partners of a $K^\pi = 2^+$, γ-vibrational band [12,16,17]. Only the two lowest levels of each band (2^+ at 1199 keV and 4^+ at 1408 keV for band 7, and 3^+ at 1291 keV and 5^+ at 1557 keV for band 8) were known prior to this study. In this work, these bands were observed up to $I^\pi = 13^+$ and 14^+, respectively. While the in-band transitions are very weak, strong out-of-band transitions to the ground state band are seen from almost every level of the bands up to the highest spins observed.

A significant fraction of these out-of-band transitions appear in the spectra in a region where the strong 1313-keV $2^+ \rightarrow 0^+$ transition in ^{136}Xe creates a broad pedestal-like background from about 1.2 to 1.4 MeV. This occurs because these spectra were corrected for Doppler shifts assuming that the transitions originate from a recoiling Hf nucleus, which

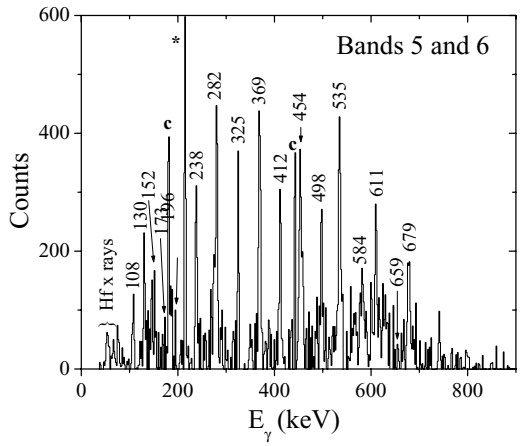

FIG. 6. Summed coincidence spectra double-gated on transitions in bands 5 and 6 of ^{180}Hf. Transitions in the GSB are marked with a (*) and contaminants with a (c).

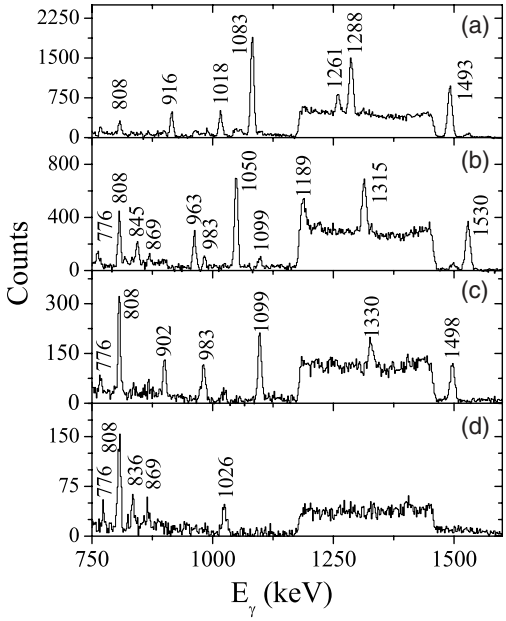

FIG. 7. Differences of spectra double-gated on consecutive γ rays in the ground state band. The pedestal feature in the 1.2–1.4 MeV region is the broadened peak from the 1313-keV $2^+ \rightarrow 0^+$ transition in ^{136}Xe (see text). (a) [215-keV/332-keV]−[332-keV/443-keV], (b) [332-keV/443-keV]−[443-keV/547-keV], (c) [443-keV/547-keV] −[547-keV/643-keV], (d) [547-keV/643-keV]−[643-keV/731-keV], highlighting transitions feeding the 6^+, 8^+, 10^+, and 12^+ states of the GSB, respectively.

sharpens Hf lines and broadens Xe lines. Clean coincidence conditions, however, can simplify the spectra even in the presence of such unusual background features. For example, differences of spectra double-gated on consecutive ground state band members are able to separate out specific subsets of γ rays which directly feed the different levels in the ground state band (Fig. 7).

For band 7, the DCO ratios of 1.01–1.07 for the 1415-, 1493-, 1530-, and 1498-keV transitions, which depopulate the newly observed higher-lying members of the band to the 4^+, 6^+, and 8^+ members of the GSB, are consistent with $\Delta I = 2$ assignments. Together with $\Delta I = 1$ transitions depopulating the band 7 members (1083 and 1050 keV, with DCO ratios of 0.72 and 0.69, respectively), the even-spin and positive-parity assignment for the bandhead is robust and consistent with previous firm spin-parity assignments to the low-spin members of this band from different measurement techniques [12,17]. For band 8, DCO ratios for the transitions depopulating the higher band members to corresponding GSB members indicate $\Delta I = 1$ stretched dipole character (0.62 for both the 1288- and 1315-keV transitions depopulating the 1928- and 2398-keV levels, respectively). These values are consistent with odd-spin assignments for the band members, and agree with previous spin-parity assignments of 3^+ and 5^+, respectively, for the 1291- and 1557-keV levels. The low intensity of the in-band $E2$ transitions in both bands 7 and 8 preclude DCO ratio measurements.

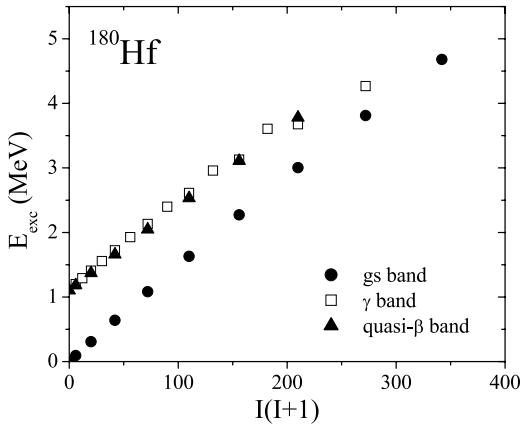

FIG. 8. Excitation energy as a function of $I(I+1)$ for $K^\pi = 0^+, 2^+$ bands.

6. Band 9

The assignments of spin and parity for band 9 are based on a measured DCO ratio of 1.05 for the 1018-keV transition to the 4^+ member of the GSB, which suggests either an $E2$ multipolarity or an unstretched $I \rightarrow I$ transition. The latter is preferred, since the $E2$ choice would make the 1658-keV level an $I^\pi = 8^+$ state, forcing the 1350-keV branch from this state to the 4^+ state of the GSB to be an improbable $E4$ transition. The five other transitions from this band to other members of the GSB were too weak for any complementary DCO information. With the 1018-keV transition as an unstretched dipole, the 1658-keV level is assigned a spin-parity of 6^+, with stretched quadrupole character for the higher in-band transitions. With this assignment, the excitation energies as a function of $I(I+1)$ for this band fit smoothly to those of a band previously reported [12] up to a 1370-keV $I^\pi = 4^+$ level, built on the first excited $(I^\pi, K) = (0^+, 0)$ state (Fig. 8). Band 9, therefore, is considered to be an extension of the earlier band built on an excited 0^+ state, which has been observed up to $I^\pi = 14^+$ in this work.

7. Band 10

Band 10 is reported for the first time. DCO ratios were difficult to measure for the transitions in this weak band. The strongest decay out from the bottom of the band is a 1261-keV γ ray, the energy of which is within 2 keV of a similar decay out from the bottom of band 11. The decay from the lowest observed 1901-keV level of this band to the 6^+ member of the GSB, together with similar decays from the higher members of the band to the corresponding higher members of the GSB, suggests a typical $E2$ sequence connecting members of the band. The 3299-keV level of this band is seen to have three decay branches, two to the 12^+ and 10^+ levels of the GSB and one to the 10^+ level of band 7, the even-spin sequence of the γ-vibrational band. This narrows the possible spin of the 3299-keV level to either 11 or 12, with a consequent spin of either 9 or 10 for the immediately lower 2729-keV level of this band. A spin assignment of 10 for the 2729-keV level is arrived at from the observation of

a 597-keV decay branch to the 2132-keV 8^+ level of band 7. The only measurable DCO ratio of 0.91 for the 1098-keV transition connecting the 2729-keV level of this band to the 10^+ level of the GSB is consistent with that expected for an $I \rightarrow I$ transition. While the above information may seem inadequate for firm spin-parity assignments for this band, the interactions of this band with band 7, the even-spin signature branch of the γ-vibrational band, as discussed in the following section, strongly supports the tentative assignments of even spins and positive parity for this band. The strong depopulation of the band to the GSB makes it difficult to ascertain if the bandhead is reached at the lowest levels observed in the sequence, but it is suggestive of a low-K vibrational character.

8. Band 11

Band 11 is also observed for the first time. Strong out-of-band transitions to the GSB, similar to band 10, are again suggestive of low-K vibrational character. As mentioned above, DCO ratios were difficult to measure for bands 10 and 11, especially since the strongest decays from the bottom of their respective sequences consist of a closely spaced doublet with energies of 1261 and 1263 keV, populating the 6^+ state of the GSB. The 1263-keV transition depopulating the lowest observed 1903-keV level of band 11 is stronger than the 1261-keV transition depopulating band 10. The absence of two decay branches from any of the levels in this band to consecutive even-spin members of the GSB suggests odd spins for the members of band 11, but the experimental information is inadequate for further discussion of this band.

B. Band structures in ^{182}Hf

The level scheme of ^{182}Hf deduced from the present work is shown in Fig. 9, where eight new transitions have been assigned. Figure 10 shows a spectrum of the GSB, obtained from the sum of double-gated coincidences. The GSB, previously known up to $I^\pi = 8^+$ [1], has been extended to $I^\pi = 18^+$ at 4733 keV. The rotational band built on the 1173-keV $I^\pi = 8^-$ isomeric state ($t_{1/2} = 61.5$ min) has been extended from 12^- to 14^-. The population of the GSB in ^{182}Hf is ~0.5% relative to the GSB of ^{180}Hf. Energies, relative γ-ray intensities, normalized to 1000 for the 224-keV $4^+ \rightarrow 2^+$ transition, and multipolarity assignments for transitions in ^{182}Hf are listed in Table II. The low statistics did not allow reliable DCO ratios to be extracted.

IV. DISCUSSION

A. Band configurations in ^{180}Hf

Nucleon orbital configurations for multiquasiparticle band structures were assigned in the framework of the cranked shell model (CSM) [18,19], by comparing alignments and Routhians extracted from the measurements with values expected for specific configurations. The "expected" values were obtained by summing the constituent single-nucleon contributions for these quantities, extracted from experimental

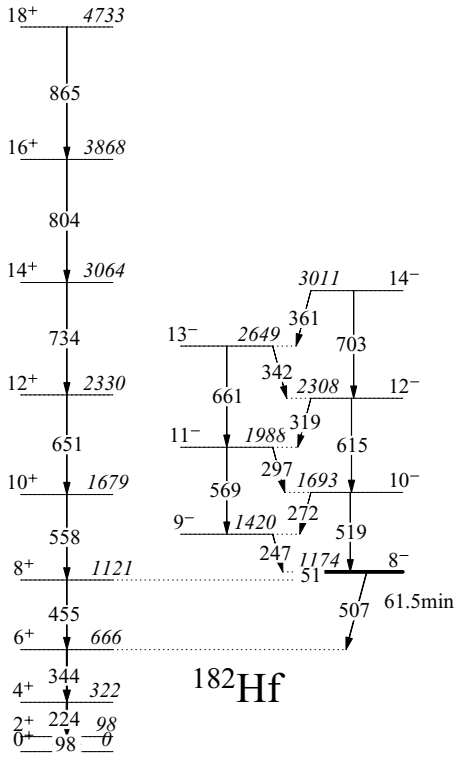

FIG. 9. Decay scheme of ^{182}Hf deduced from this work. All energies are in keV.

data in neighboring odd-A nuclei. In addition, g factors extracted from in-band $M1/E2$ branching ratios for high-K bands were compared with theoretical values expected for the possible configurations (Table III), as described below. Experimental bandhead energies were also compared with theoretical calculations [20], where appropriate.

Figure 11 shows the plots for experimental Routhians and alignments for the high-K bands observed in ^{180}Hf, and comparison with experimental values from odd-A neighbors. The Harris parameters [21], $\mathcal{J}_0$ ($32\hbar^2$ MeV^{-1}) and $\mathcal{J}_1$

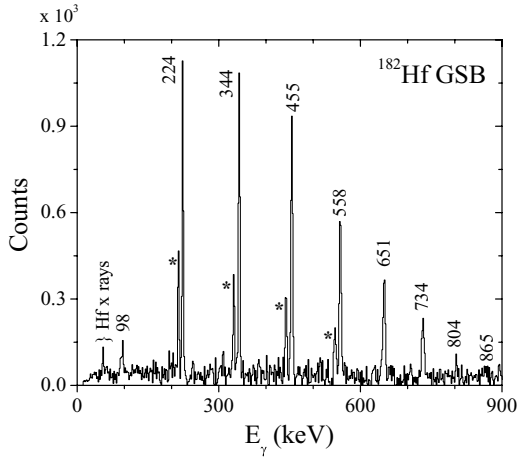

FIG. 10. Summed coincidence spectra double-gated on transitions in the ground state band of ^{182}Hf. Contaminants from the GSB transitions in the strong ^{180}Hf channel are marked with (*).

TABLE II. Energies, initial and final states, and relative γ-ray intensities for the γ-ray transitions observed in ^{182}Hf. The uncertainties in the transition energies are $\sim \pm 0.5$ keV.

E_γ(keV)	Band$_i$ $\rightarrow$ Band$_f$	E_i(keV)	$I_i^\pi \rightarrow I_f^\pi$	I_γ
51.5	2 $\rightarrow$ GSB	1173	$8^- \rightarrow 8^+$	
98.3	GSB $\rightarrow$ GSB	98	$2^+ \rightarrow 0^+$	
224.1	GSB $\rightarrow$ GSB	322	$4^+ \rightarrow 2^+$	1000(32)
246.8	1 $\rightarrow$ 2	1420	$9^- \rightarrow 8^-$	201(14)
272.3	2 $\rightarrow$ 1	1692	$10^- \rightarrow 9^-$	143(12)
296.6	1 $\rightarrow$ 2	1989	$11^- \rightarrow 10^-$	182(13)
319.2	2 $\rightarrow$ 1	2307	$12^- \rightarrow 11^-$	184(14)
341.6	1 $\rightarrow$ 2	2649	$13^- \rightarrow 12^-$	155(12)
343.7	GSB $\rightarrow$ GSB	666	$6^+ \rightarrow 4^+$	700(26)
360.5	2 $\rightarrow$ 1	3010	$14^- \rightarrow 13^-$	193(14)
455.4	GSB $\rightarrow$ GSB	1121	$8^+ \rightarrow 6^+$	355(19)
507.1	2 $\rightarrow$ GSB	1173	$8^- \rightarrow 6^+$	123(11)
518.9	2 $\rightarrow$ 2	1692	$10^- \rightarrow 8^-$	113(11)
558.2	GSB $\rightarrow$ GSB	1679	$10^+ \rightarrow 8^+$	249(16)
569.1	1 $\rightarrow$ 1	1989	$11^- \rightarrow 9^-$	178(13)
615.0	2 $\rightarrow$ 2	2307	$12^- \rightarrow 10^-$	205(14)
651.4	GSB $\rightarrow$ GSB	2330	$12^+ \rightarrow 10^+$	182(13)
661.0	1 $\rightarrow$ 1	2649	$13^- \rightarrow 11^-$	143(12)
703.0	2 $\rightarrow$ 2	3010	$14^- \rightarrow 12^-$	150(12)
733.6	GSB $\rightarrow$ GSB	3064	$14^+ \rightarrow 12^+$	140(12)
803.9	GSB $\rightarrow$ GSB	3868	$16^+ \rightarrow 14^+$	118(11)
864.7	GSB $\rightarrow$ GSB	4733	$18^+ \rightarrow 16^+$	87(9)

($37\hbar^4$ MeV^{-3}), were chosen to keep the alignment and Routhians approximately constant for the GSB at the lowest spins. Routhians and alignments were calculated from available experimental data on the low-lying single-particle orbitals of the odd-A neighbors of ^{180}Hf (^{179}Lu, ^{179}Hf, ^{181}Hf, and ^{181}Ta). The data from odd-A neighbors on either side were averaged when available and compared with those of ^{180}Hf side bands. For the odd-N ^{179}Hf [22] and ^{181}Hf [1,2,23], the Nilsson orbitals associated with observed single-quasiparticle (single-qp) states are $[615]\frac{11}{2}^+$, $[624]\frac{9}{2}^+$, $[514]\frac{7}{2}^-$, $[512]\frac{5}{2}^-$, $[510]\frac{1}{2}^-$, and $[521]\frac{1}{2}^-$. For the odd-Z ^{179}Lu [12] and ^{181}Ta [24], the relevant orbitals are $[514]\frac{9}{2}^-$, $[404]\frac{7}{2}^+$, and $[402]\frac{5}{2}^+$. Alignments obtained from odd-A neighbors can be summed and compared with experimental two-quasiparticle bands in even-even nuclei without any further adjustable parameters. To compare the Routhian of a two-quasiparticle band in this manner, a pairing energy term needs to be added to the summed odd-A contribution. A value of 1.2 MeV for the pairing energy

TABLE III. Two-quasiparticle configuration assignments in ^{180}Hf, where the average experimental value of $|\frac{g_K - g_R}{Q_0}|$ for each band is compared with the expected value for the assigned configuration.

K^π	Configuration	$\lvert\frac{g_K-g_R}{Q_0}\rvert_{\rm exp}$	$(\frac{g_K-g_R}{Q_0})_{\rm calc}$
4^-	$\nu^2[624]\frac{9}{2}^+ \otimes [510]\frac{1}{2}^-$	0.03(1)	-0.04
6^+	$\pi^2[404]\frac{7}{2}^+ \otimes [402]\frac{5}{2}^+$	0.09(1)	0.10
8^-	$\pi^2[404]\frac{7}{2}^+ \otimes [514]\frac{9}{2}^-$	0.10(1)	0.10

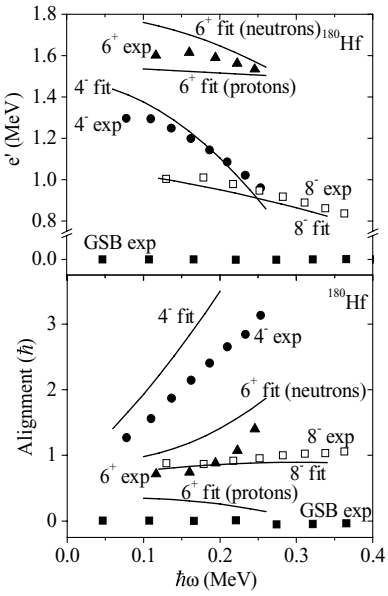

FIG. 11. Experimental Routhians and alignments for bands in ^{180}Hf, compared with summed single-particle contributions extracted from data on odd-A neighbors. Harris parameters $\mathcal{J}_0(32\hbar^2\,\mathrm{MeV}^{-1})$ and $\mathcal{J}_1(37\hbar^4\,\mathrm{MeV}^{-3})$ have been used.

was found to provide excellent agreement of the Routhians for all three two-quasiparticle configurations analyzed.

The magnitude of the in-band quadrupole/dipole mixing ratio, δ, is obtained from the quadrupole admixture q, given by

$$q = \frac{\delta^2}{1+\delta^2} = \frac{2K^2(2I-1)}{(I+1)(I+K-1)(I-K-1)} \left(\frac{E_1}{E_2}\right)^5 \frac{T_2}{T_1}. \quad (2)$$

The subscripts 1,2 refer to $\Delta I = 1, 2$ transitions, respectively. $E_{1,2}$ are the γ-ray energies (in MeV), $T_{1,2}$ the corresponding intensities, and I the spin of the initial level.

The relation between g_K and g_R, the intrinsic and rotational g factors, and δ is

$$\left|\frac{g_K - g_R}{Q_0}\right| = 0.933 \frac{E_1}{\delta\sqrt{I^2-1}}, \quad (3)$$

where Q_0 (in e b) is the intrinsic quadrupole moment. Typical values for the $A \sim 180$ mass region of $g_R \approx 0.28$ and $Q_0 \approx 7$ e b [1,2] were used. The g_K value for an orbital with the asymptotic Nilsson quantum numbers $\Omega^\pi[Nn_z\Lambda]$ is estimated from the relation

$$Kg_K = \sum(\Lambda g_\Lambda + 0.6\Sigma g_\Sigma), \quad (4)$$

where Λ and Σ are the projections of the nucleon orbital and spin angular momenta, respectively, with $\Omega = \Lambda \pm \Sigma$. The corresponding g factors are $g_\Lambda = 0$ and 1, and $g_\Sigma = -3.83$ and 5.59, for neutrons and protons, respectively. A typical spin quenching factor of 0.6 [25] was used for the estimates.

The high-K bands 1 through 6, the quadrupole vibrational bands 7 through 9, and the ground state band are discussed separately below. Configuration assignments for bands 10 and

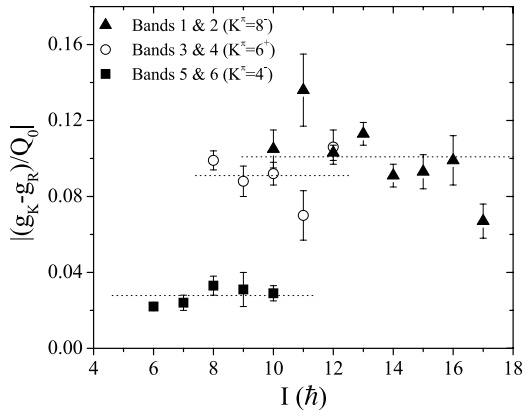

FIG. 12. Experimental $|\frac{g_K-g_R}{Q_0}|$ ratios for two-quasiparticle excitations in ^{180}Hf. Horizontal dashed lines denote the average experimental value for each band.

11 were not attempted because of insufficient spectroscopic data.

B. High-K band structures

1. Bands 1 and 2

Bands 1 and 2, built on the 1141-keV $I^\pi = 8^-$, $t_{1/2} = 5.5$ hr isomeric level were previously assigned a two-quasiproton $\pi^2[404]\frac{7}{2}^+ \otimes [514]\frac{9}{2}^-$ configuration [1]. The experimental alignments and Routhians extracted with the extended data from the present work show almost no signature splitting, consistent with expectations for a high-K band, and are in excellent agreement with the expected values for this configuration (Fig. 11). This configuration assignment is also corroborated by an experimental $|\frac{g_K-g_R}{Q_0}|$ value of 0.10(1) (Fig. 12), compared with the expected value of 0.10 (Table III). While two possible two-quasineutron configurations $\nu^2[624]\frac{9}{2}^+ \otimes [514]\frac{7}{2}^-$ and $\nu^2[615]\frac{11}{2}^+ \otimes [512]\frac{5}{2}^-$ can form an $I^\pi = 8^-$ state, these are discarded on the basis of excitation energy and g-factor arguments. The $|\frac{g_K-g_R}{Q_0}|$ values for the $\nu^2[624]\frac{9}{2}^+ \otimes [514]\frac{7}{2}^-$ and $\nu^2[615]\frac{11}{2}^+ \otimes [512]\frac{5}{2}^-$ are 0.04 and 0.08, respectively. Blocked-BCS calculations [20] for the two-quasiproton configuration ($E_{\rm calc} = 1128$ keV) are in excellent agreement with experiment, while the quasineutron configurations are predicted to lie more than a MeV higher in excitation energy.

2. Bands 3 and 4

Bands 3 and 4 are built on the 1702-keV $I^\pi = 6^+$ level. There are two possible low-lying configurations for an $I^\pi = 6^+$ state, $\pi^2[404]\frac{7}{2}^+ \otimes [402]\frac{5}{2}^+$ and $\nu^2[514]\frac{7}{2}^- \otimes [512]\frac{5}{2}^-$. The excitation energies for the two configurations are very similar. The experimental alignments lie in between the values expected for the two configurations at the lower rotational frequencies (Fig. 11). The experimental $M1/E2$ branching ratios (Fig. 12), however, result in a $|\frac{g_K-g_R}{Q_0}|$ value of 0.09(1) (Table III). The corresponding calculated values are 0.04 and 0.10 for $\nu^2[514]\frac{7}{2}^- \otimes [512]\frac{5}{2}^-$ and $\pi^2[404]\frac{7}{2}^+ \otimes [402]\frac{5}{2}^+$, respectively. It should be noted that alignment information on proton orbitals was only available from the higher-Z Ta neighbor, since very little band structure information is known in the lower-Z Lu neighbor. The alignment values are also somewhat sensitive to the Harris parameters. More emphasis is placed on the g-factor measurements, which favor the $\pi^2[404]\frac{7}{2}^+ \otimes [402]\frac{5}{2}^+$ configuration assignment, in agreement with earlier work [13], where the assignment is shown to fit the energy and alignment systematics of this two-quasiproton excitation in the neighboring lighter hafnium isotopes very well. Nevertheless, the possibility of admixtures of the neutron configuration mentioned above cannot be entirely ruled out.

3. Bands 5 and 6

Bands 5 and 6, built on the 1374-keV $I^\pi = 4^-$ level, were previously assigned as signature partners of the configuration $\nu^2[624]\frac{9}{2}^+ \otimes [510]\frac{1}{2}^-$ [13]. This is the configuration with the highest alignment observed in ^{180}Hf (Fig. 11). Again, the experimental alignments agree well with values expected for this configuration. The extracted $|\frac{g_K-g_R}{Q_0}|$ value of 0.3(1) from the measured in-band branching ratios (Fig. 12) agrees very well with the expected value of 0.4 for this configuration (Table III). Although the maximum spin for this configuration is $I^\pi = 5^-$, residual spin-spin interactions are estimated to favor the $I_{\rm max} - 1$ state by ~300 keV. Multiquasiparticle calculations including spin-spin residual interactions reproduce the excitation energy of this state within ~30 keV. Energy considerations exclude the choice of a $[521]\frac{1}{2}^-$ orbital over the $[510]\frac{1}{2}^-$ orbital, both of which result in an identical g factor. The latter is expected to be the lower energy configuration in this nucleus, since it lies ~240 keV lower in ^{179}Hf and is the ground state in the ^{181}Hf nucleus. The spin-spin interactions involving the $[521]\frac{1}{2}^-$ orbital leading to a 4^- level would also be energetically unfavorable.

C. Quadrupole vibrational bands and low-K structures in ^{180}Hf

Bands 7, 8, and 9 have the characteristics of one-phonon vibrational excitations. Multiple decays are observed in ^{180}Hf from higher-lying states in bands 7, 8, and 9 to levels in the ground state band (Fig. 2) over an extended range of spin. In addition, the locus of level energies of these bands as a function of $I(I+1)$ is approximately parallel to that of the GSB, demonstrating very similar effective moments of inertia (Fig. 8). These are characteristic signatures of vibrational excitations. Bands 7 and 8, built on a 2^+ state, are signature partners and have the characteristics of a γ-vibrational band, while band 9, built on a 0_2^+ state, is characterized as a quasi-β band, since an accurate characterization of β bands is difficult [26].

The robustness of the γ-vibrational band up to spin 10 was investigated by comparing measured branching ratios of the transitions linking the γ band to the GSB with Alaga intensity rules [27,28]. The branching ratio of the strengths of the two

TABLE IV. Comparison of experimental branching ratios of the γ-vibrational band with Alaga predictions (see text for details).

I_i	3	4	5	6	7	8	10
R_{Alaga}	0.40	3.0	0.57	3.7	0.67	4.2	4.5
R_{exp}	0.49(4)	4.1(4)	0.63(6)	3.7(2)	0.58(3)	3.8(1)	3.5(7)

transitions depopulating the same initial level of a vibrational band to two consecutive levels of the GSB has been defined as

$$R_{\text{branching}} = \frac{B(E2 : I_i \rightarrow I_g)}{B(E2 : I_i \rightarrow I_g - 2)}, \quad (5)$$

where I is the spin of the level, and subscripts i and g denote initial and GSB levels, respectively. As shown in Table IV, the experimental branching ratios for bands 7 and 8 are in fair agreement with the Alaga predictions, supporting their assignment as signature partners of the γ band.

Above spin 10, a strong odd-even staggering or signature splitting for the γ band in ^{180}Hf is observed. This is highlighted in Fig. 13(a), in which the staggering index $S(I)$, defined as [29]

$$S(I, I-1, I-2) = \frac{2(E_I - E_{I-1}) - (E_I - E_{I-2})}{E(2_1^+)} \quad (6)$$

(where E_I is the excitation energy of the γ-band level with angular momentum I), is plotted as a function of I. A dramatic increase in the staggering is observed as a function of increasing spin in ^{180}Hf. This behavior is contrasted with the neighboring ^{178}Hf nucleus, in which the γ band has also been recently extended to high spins [30], and a small odd-even staggering is observed to stay fairly constant up to spin 16. While typical discussions of odd-even staggering in γ-vibrational bands revolve around possibilities of γ softness or triaxiality, there seems to be a rather straightforward explanation in this particular case, arising from the mixing of the even-spin signature of the band with another at intermediate spins, with an interchange of character at the highest spins observed. This is illustrated in Fig. 13(b), where the energies of bands 7 and 8 (the γ-band members of even and odd spin, respectively) are compared with those of band 10 as a function of $I(I+1)$ with an arbitrary rigid-rotor reference subtracted. Such plots highlight deviations from smooth behavior that are typically indicative of band interactions. The interaction between bands 7 and 10 is evident from this plot. The observation of two transitions from consecutive members of band 10 to the 8^+ and 10^+ levels of the γ-vibrational band solidifies the evidence for the mixing scenario and provides additional support and consistency to the tentative spin and parity assignments for this band. The observation of the 1669-keV transition from the 3299-keV level of band 10 to the 10^+ level of the GSB lends further credence to this interpretation. The proposed explanation of the "apparent" signature splitting of the γ-vibrational band, therefore, is that the even-spin signature of the band crosses, interacts, and changes character with a low-K two-quasiparticle band around spin 10. Microscopic analyses can point to the dominance of specific two-quasiparticle components in the structure of the γ-vibrational wave function. Early calculations for this nucleus within the framework of the Nilsson model [31] ascribe 81% of the γ-vibrational wave function to neutrons, with contributions from the $\nu^2[514]\frac{7}{2}^- \otimes [512]\frac{3}{2}^-$, $\nu^2[510]\frac{1}{2}^- \otimes [512]\frac{3}{2}^-$, and $\nu^2[510]\frac{1}{2}^- \otimes [512]\frac{5}{2}^-$ configurations dominating with 27%, 27%, and 23%, respectively.

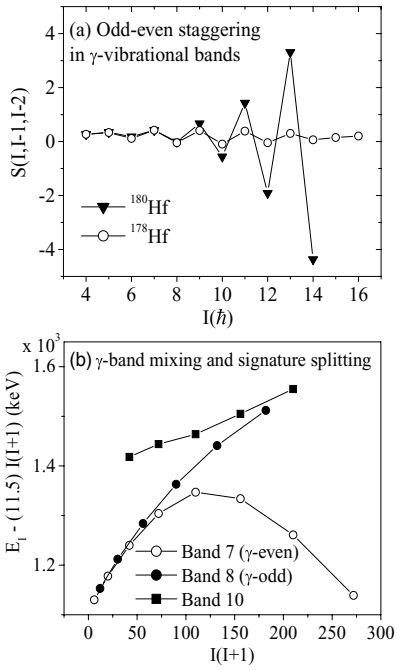

FIG. 13. (a) Staggering indices for ^{178}Hf and ^{180}Hf (see text for details). (b) Level energies, with a constant rigid rotor contribution subtracted, for the γ band and band 10 in ^{180}Hf.

D. Crossing frequencies and shape evolution in ^{180,182}Hf

One of the more interesting results from the present data of rotational excitations in ^{180}Hf and ^{182}Hf is the observation of a significantly higher alignment frequency of the first nucleon pairs in both nuclei, compared with the lighter even-N isotopes [Fig. 14(a)]. While the $N = 90$–106 isotopes exhibit a first crossing at a frequency $\hbar\omega < \sim 0.3$ MeV, almost no gain in alignment is observed for ^{180,182}Hf up to $\hbar\omega \approx 0.43$ MeV. Delayed alignments have experimentally been observed in the corresponding W ($Z = 74$) [32,33] and Os ($Z = 76$) isotones [Figs. 14(b) and 14(c)]. In W nuclei, while $N < 106$ isotopes align at $\hbar\omega < \sim 0.3$ MeV, a sharp alignment is observed at $\hbar\omega \approx 0.38$ MeV in ^{182}W ($N = 108$) [33]. In ^{184}W ($N = 110$), the ground state band has been observed up to $\hbar\omega \approx 0.4$ MeV, where an onset of alignment is seen. For the isotones in Os, the first alignment has been completely mapped and reveals a strong backbending behavior. The alignments in ^{184,186}Os ($N = 108, 110$) are seen at $\hbar\omega \approx 0.35$ MeV, which is considerably higher than lighter isotopes which align at $\hbar\omega \approx 0.25$ MeV. The experimental crossing frequencies in the osmium isotopes are lower than those in the corresponding hafnium and tungsten isotones by ~0.05 MeV, but the γ softness inherent in the Os isotopes complicates a direct comparison with the Hf and W nuclei. The absence of obvious

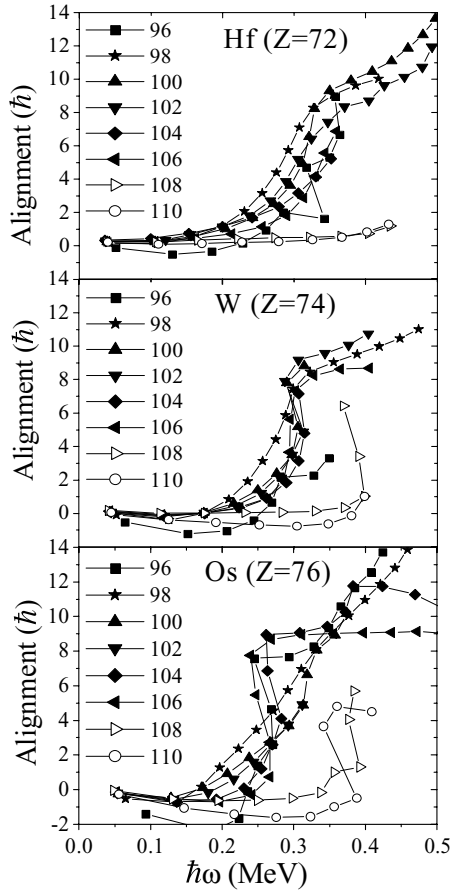

FIG. 14. Alignment systematics of even-$N(N = 96–110)$ (a) hafnium ($Z = 72$), (b) tungsten ($Z = 74$), and (c) osmium ($Z = 76$) isotopes. The same Harris parameters, $\mathcal{J}_0(30\hbar^2\,\mathrm{MeV}^{-1})$ and $\mathcal{J}_1(40\hbar^4\,\mathrm{MeV}^{-3})$, have been used for all plots.

nucleon alignment in the ground state bands for both ^{180}Hf and ^{182}Hf up to rotational frequencies of $\hbar\omega \sim 0.43$ MeV suggests that either the nucleons align at a higher frequency or sharp backbends are imminent, which would effectively reduce the crossing frequency to below 0.43 MeV.

Previous calculations with a modified harmonic oscillator potential [34] predict that the first $i_{13/2}$ neutron alignment is considerably delayed for the $N = 108$ isotones compared with that for the lighter ones. Cranked Woods-Saxon calculations have been performed to investigate the predicted crossing frequencies and shape evolution with increasing rotational frequency and spin [35], which were compared with experimental results. The universal Woods-Saxon potential parameters [36], with the Hartree-Fock-Bogoliubov (HFB) formalism and Strutinsky shell correction were used. The pairing interaction was taken to be of the monopole form. To calculate the total Routhian surfaces (TRS), the pair gap Δ_0 was determined self-consistently at $\omega = 0$ using the BCS formalism and was allowed to decrease gradually to half its value at $\omega = \omega_c$. The value of ω_c was chosen to be 0.7 MeV, which is typical for the rare-earth region. For determining crossing frequencies, an empirical value of the pair gap energy was obtained from odd-even mass differences using a five-point expression [37].

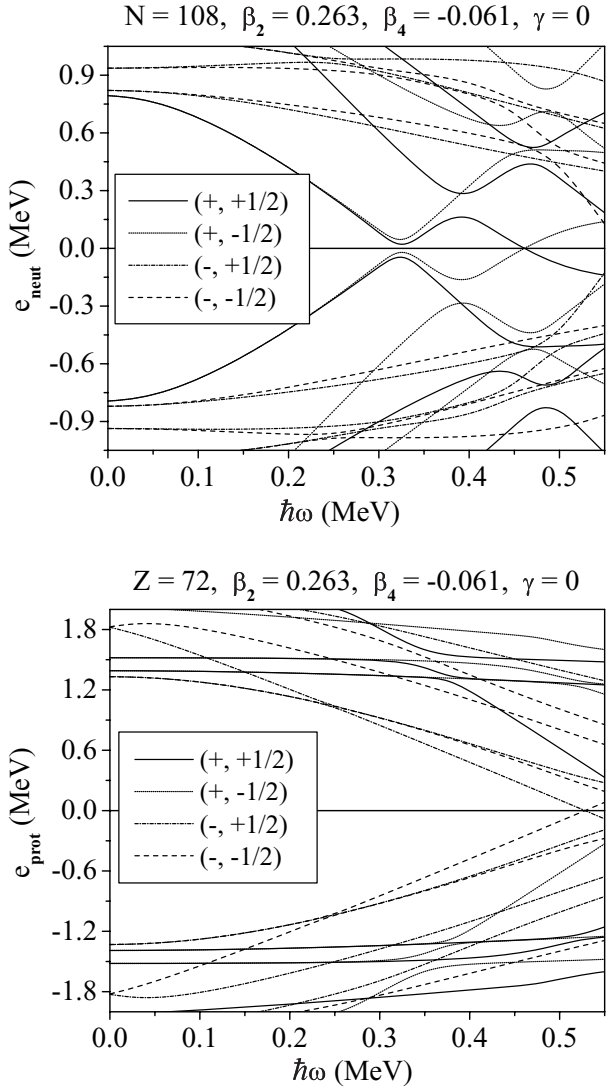

FIG. 15. Calculated neutron and proton quasiparticle energy levels for ^{180}Hf [35].

The calculated quasiparticle levels for ^{180}Hf ($N = 108$) are shown in Fig. 15. The first crossing, corresponding to the first $i_{13/2}$ neutron alignment, is seen to occur, with very weak interaction, at $\hbar\omega = 0.33$ MeV, a small jump over the crossing frequencies of ~0.26 MeV calculated for the $N = 100$ to $N = 106$ even-N Hf isotopes [35]. For ^{182}Hf ($N = 110$), the first calculated crossing is at 0.38 MeV (Fig. 16). The calculations indicate that the interaction matrix element at the crossing, as a function of N, is the smallest for $N = 108$. The observed alignment is, therefore, expected to be most pronounced for the $N = 108$ isotones, as is indeed observed [33] in ^{182}W [Fig. 14(b)]. The calculations for ^{182}W predict the crossing at $\hbar\omega = 0.34$ MeV. The experimentally observed value for ^{182}W is $\hbar\omega = 0.38$ MeV, while the first crossing is observed at 0.29 MeV for ^{180}W. The increase in the crossing frequencies for $N = 108$ isotones in this region is generally attributed to an increased gap near the Fermi level, a consequence of a neutron subshell closure at $N = 108$ [32]. This subshell closure, which has been predicted from earlier studies [16],

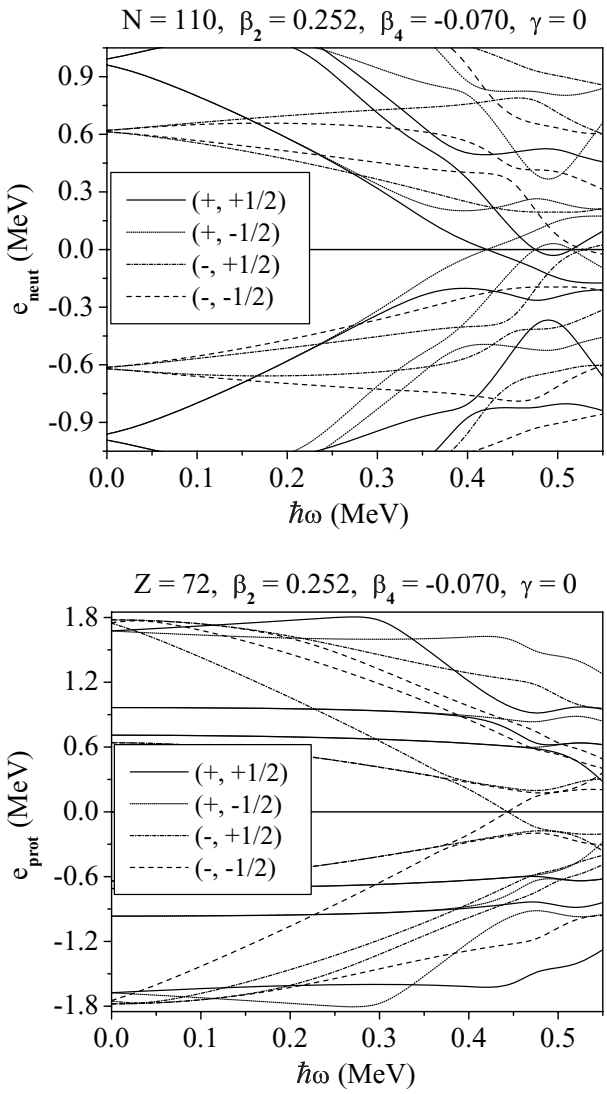

FIG. 16. Calculated neutron and proton quasiparticle energy levels for ^{182}Hf [35].

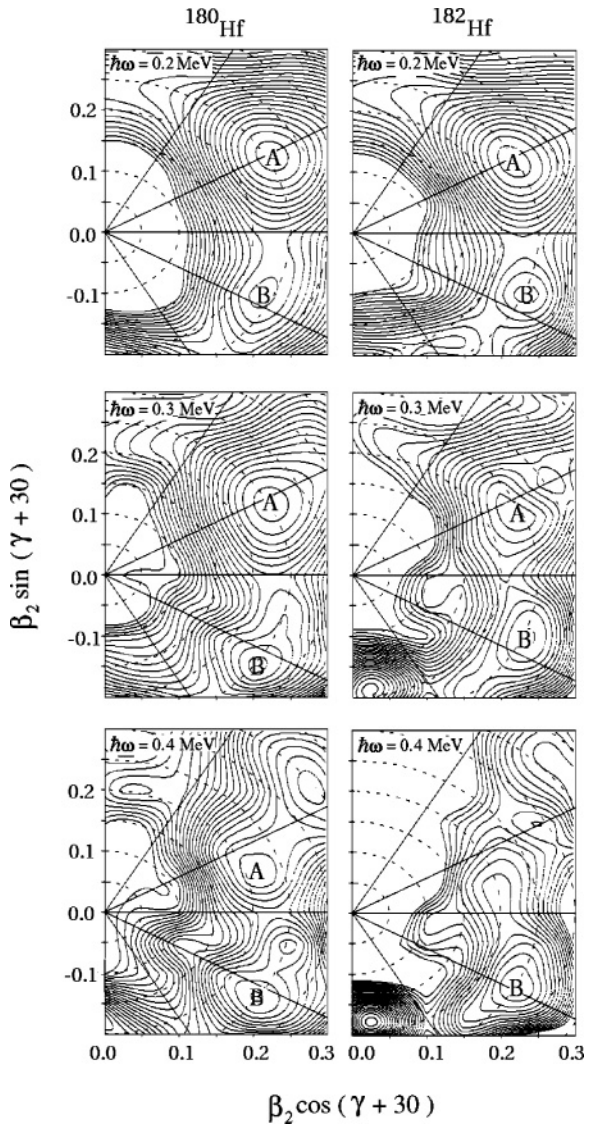

FIG. 17. Total Routhian surfaces (TRS) calculated [35] for ^{180,182}Hf, at $\hbar\omega$ values of 0.2, 0.3, and 0.4 MeV. Contours are separated by 0.25 MeV. Energy minima show a drift from prolate (A) to oblate (B) shapes as a function of rotational frequency. For the same rotational frequency, the oblate energy minimum in ^{182}Hf is better defined than in ^{180}Hf.

is also evident from an increase in the experimental odd-even mass differences [38]. The modified oscillator calculations reproduce the subshell gap at $N = 108$ better than the Woods-Saxon calculations. Therefore, the crossing frequency, which increases in the vicinity of a shell gap, is predicted to be higher by the modified oscillator calculations.

Another intriguing possibility is whether the discrepancies between expected and observed crossing frequencies for ^{180,182}Hf are related to the predicted collective prolate-to-oblate shape transitions at high spin for the $N \geqslant 108$ even-N isotones [4,5,39]. The spin values at which the shape transition is predicted is $\sim 26\hbar$ for ^{180}Hf [4] and $\sim 22\hbar$ for ^{182}Hf [5]. TRS calculations [35] for the global energy minima in even-N Hf isotopes indicate that the oblate minimum appears at progressively lower energy with increasing neutron number and becomes yrast for $N \geqslant 108$ nuclei at higher frequencies (Fig. 17). These results are in good agreement with those of Xu *et al.* [5]. The present work extends the ground state band of ^{182}Hf up to $18\hbar$ and rotational frequencies of $\sim$0.4 MeV, in the vicinity of the predicted prolate-to-oblate shape transition. It is suggested that the collective oblate shapes result mainly from the rotational alignments of the $i_{13/2}$ neutron and $h_{11/2}$ proton pairs [5]. The weak band that interacts with the even signature of the γ-vibrational band seems headed toward a crossing with the ground state band in the vicinity of the first nucleon alignment. Since these alignments have yet to be experimentally mapped, a detailed discussion on the possible effects of a shape change on nucleon alignments and vice versa seems premature.

V. CONCLUSIONS

The present work has significantly expanded our knowledge of high-spin collective structures in neutron-rich hafnium

nuclei, using recent advances in experimental techniques and the combination of powerful detector systems. The ground state bands of ^{180}Hf and ^{182}Hf have been extended close to their respective first nucleon alignments. Configurations for observed two-quasiparticle, high-K structures have been firmly established. A notable result is the absence of alignment in either nucleus up to the highest spins achieved in this work, which constitutes a significant increase in the frequency of the first crossing compared to the lower-A even-even isotopes. Similar behavior observed in the $N = 108$ and $N = 110$ isotones of W and Os nuclei is attributed to a subshell closure leading to an increased pair gap. Increasing odd-even staggering in γ-vibrational excitations mapped to moderately high angular momenta in ^{180}Hf is understood via the interaction of the even-spin signature of the band with a low-K two-quasiparticle band. Systematic cranked shell model calculations have been performed to understand the possible parameters which might affect nucleon alignment characteristics in these nuclei which lie at the edge of current experimental techniques. The exercise highlights the inadequacy of multipoint smoothing algorithms used to extract pair gap parameters near subshell closures. The determination of any possible connection between the delayed alignment and predicted prolate-to-oblate shape transitions at higher spin must await further data. A recent experiment with a heavier reaction partner for hafnium at a higher bombarding energy should be able to map the high-spin structures of these nuclei beyond the first nucleon alignments.

ACKNOWLEDGMENTS

This work was supported by the U.S. Department of Energy under Grants DE-FG02-94ER40848, W-31-109-ENG-38, and the National Science Foundation.

[1] R. D'Alarcao *et al.*, Phys. Rev. C **59**, R1227 (1999).
[2] I. Shestakova *et al.*, Phys. Rev. C **64**, 054307 (2001).
[3] S. Åberg, Nucl. Phys. **A306**, 89 (1978).
[4] R. R. Hilton and H. J. Mang, Phys. Rev. Lett. **43**, 1979 (1979).
[5] F. R. Xu, P. M. Walker, and R. Wyss, Phys. Rev. C **62**, 014301 (2000).
[6] R. Broda, M. A. Quader, P. J. Daly, R. V. F. Janssens, T. L. Khoo, W. C. Ma, and M. W. Drigert, Phys. Lett. **B251**, 245 (1990); I. Y. Lee *et al.*, Phys. Rev. C **56**, 753 (1997); C. Wheldon *et al.*, Phys. Lett. **B425**, 239 (1998).
[7] M. W. Simon, D. Cline, C. Y. Wu, R. W. Gray, R. Teng, and C. Long, Nucl. Instrum. Methods Phys. Res. A **452**, 205 (2000).
[8] H.-Q. Jin, TSCAN and related programs. A package to perform tape scanning and to manipulate matrices, RUTGERS-ORNL-UTK, 1992–1997.
[9] D. C. Radford, Nucl. Instrum. Methods Phys. Res. A **361**, 297 (1995).
[10] K. S. Krane, R. M. Steffen, and R. M. Wheeler, Nucl. Data Tables **11**, 351 (1973).
[11] A. Krämer-Flecken, T. Morek, R. M. Lieder, W. Gast, G. Hebbinghaus, H. M. Jäger, and W. Urban, Nucl. Instrum. Methods Phys. Res. A **275**, 333 (1989).
[12] *Table of Isotopes,* edited by R. B. Firestone, V. S. Shirley, C. M. Badin, S. Y. F. Chu, and J. Zipkin (Wiley, New York, 1996), Vol. 2., 8th Ed.
[13] R. D'Alarcao, Ph.D. thesis, University of Massachusetts Lowell, 2000.
[14] P. Chowdhury *et al.*, Nucl. Phys. **A682**, 65c (2001).
[15] E. Browne, Nucl. Data Sheets **52**, 127 (1987).
[16] D. G. Burke, I. Nowikow, Y. K. Peng, and J. C. Yanch, Can. J. Phys. **61**, 460 (1983).
[17] E. P. Grigor'ev, V. A. Bondarenko, and K. Nam, Sov. J. Nucl. Phys. **54**, 914 (1991).
[18] R. Bengtsson and S. Frauendorf, Nucl. Phys. **A327**, 139 (1979).
[19] S. Frauendorf, L. L. Riedinger, J. D. Garrett, J. J. Gaardhoje, G. B. Hagemann, and B. Herskind, Nucl. Phys. **A431**, 511 (1984).
[20] K. Jain, O. Burglin, G. D. Dracoulis, B. Fabricius, N. Rowley, and P. M. Walker, Nucl. Phys. **A591**, 61 (1995).
[21] S. M. Harris, Phys. Rev. B **138**, 509 (1965).
[22] S. M. Mullins, G. D. Dracoulis, A. P. Byrne, T. R. McGoram, S. Bayer, R. A. Bark, R. T. Newman, W. A. Seale, and F. G. Kondev, Phys. Rev. C **61**, 044315 (2000).
[23] V. Bondarenko *et al.*, Nucl. Phys. **A709**, 3 (2002).
[24] G. D. Dracoulis, A. P. Byrne, S. M. Mullins, T. Kibedi, F. G. Kondev, and P. M. Davidson, Phys. Rev. C **58**, 1837 (1998).
[25] P. M. Walker, G. D. Dracoulis, A. P. Byrne, B. Fabricius, T. Kibedi, A. E. Stuchbery, and N. Rowley, Nucl. Phys. **A568**, 397 (1994), and references therein.
[26] P. E. Garrett, J. Phys. G **27**, R1 (2001).
[27] A. Bohr and B. R. Mottelson, *Nuclear Structure* (Benjamin, New York, 1975).
[28] G. Alaga, K. Alder, A. Bohr, and B. R. Mottelson, Mat. Fys. Medd. Dan. Vid. Selsk. **29**, 9 (1955).
[29] N. V. Zamfir and R. F. Casten, Phys. Lett. **B260**, 265 (1991).
[30] A. B. Hayes *et al.*, Phys. Rev. Lett. **89**, 242501 (2002).
[31] D. R. Bes, P. Federman, E. Maqueda, and A. Zuker, Nucl. Phys. **65**, 1 (1965).
[32] M. P. Carpenter *et al.*, Nucl. Phys. **A513**, 125 (1990).
[33] T. Shizuma, S. Mitarai, G. Sletten, R. A. Bark, N. L. Gjorup, H. J. Jensen, J. Wrzesinski, and M. Piiparinen, Nucl. Phys. **A593**, 247 (1995).
[34] R. Bengtsson, S. Frauendorf, and F.-R. May, At. Data Nucl. Data Tables **35**, 15 (1986).
[35] S. K. Tandel *et al.* (unpublished).
[36] W. Nazarewicz, J. Dudek, R. Bengtsson, T. Bengtsson, and I. Ragnarsson, Nucl. Phys. **A435**, 397 (1985).
[37] P. Möller and J. R. Nix, Nucl. Phys. **A536**, 20 (1992).
[38] G. Audi and A. H. Wapstra, Nucl. Phys. **A595**, 409 (1995).
[39] J. Jolie and A. Linnemann, Phys. Rev. C **68**, 031301(R) (2003).